Precambrian Ophiolites and Related Rocks
Edited by Timothy M. Kusky
Developments in Precambrian Geology, Vol. 13 (K.C. Condie, Series Editor)

Chapter 13

3.0 GA OLONDO GREENSTONE BELT IN THE ALDAN SHIELD, E. SIBERIA

IGOR S. PUCHTEL

Department of the Geophysical Sciences, The University of Chicago, 5734 South Ellis Avenue, Chicago, IL 60637, USA

1. INTRODUCTION

Greenstone belts are the best preserved areas in Precambrian shields that provide a window into a distant geological past. One of the most challenging issues in the earth sciences is the reconstruction of the chemical and tectonic evolution of the early Earth. Plate tectonics is the most commonly cited mechanism by which the modern Earth releases its heat. Plate tectonics is responsible for chemical and mass exchange within the mantle and basically for the way our planet looks and evolves today. Whether the Earth was so different in the Archean that plate tectonics did not operate has remained the subject of a long-standing debate (e.g., deWit and Ashwal, 1986, 1997). This question still cannot be answered with a sufficient degree of certainty due to the fact that relicts of *bone fide* Archean oceanic crust as we understand it have yet to be found. This is mostly because of the contorted and incomplete nature of the record in the greenstone belts none of which can be regarded as an unequivocal Archean ophiolite, and also because of the highly varied ways in which plate tectonic processes can operate. But it appears that we are getting very close indeed. This manuscript is an attempt to address the above problem by studying a 3.0 billion-year-old ophiolite-like association of the Olondo greenstone belt in the Aldan shield.

The Olondo greenstone belt is a unique structure for several reasons. First, it is distinguished from the other greenstone belts in the Aldan Shield by an abundance and a great facies diversity of mafic-ultramafic rocks. In this respect, there is no match to this greenstone belt in the Aldan Shield, one of the largest cratonic segments on Earth. Second, the rocks are relatively well preserved both geologically and geochemically compared to other Archean ophiolite-like sequences worldwide, and thus can be regarded as valuable witnesses of the early history of the Earth. Third, the Olondo greenstone belt contains one of the oldest ophiolite-like sequences on the planet. Because of the reasons outlined above, this is arguably the best studied greenstone belt in the Aldan shield. In addition, the age of the Olondo greenstone belt at 3.0 Ga is intermediate between the two most commonly cited periods of global crust-forming activity, namely, 2.7 and 3.4 Ga (Condie, 1995, 1998). Thus, the study of this belt can help fill the gap in our understanding the significance of

DOI: 10.1016/S0166-2635(04)13013-2

the tectonothermal and chemical evolution of the Earth during the time period between the early and late Archean.

2. REGIONAL GEOLOGY

The Aldan Shield is the largest basement salient in the Siberian craton. The shield consists of the Aldan granulite-gneiss terrain, and Batomga and Olekma gneiss-greenstone terrains (GGT) to the west and east, respectively (Fig. 1). The geology, stratigraphy and geochronology of the region have been reviewed in numerous publications (Mironiuk et al., 1971; Drugova et al., 1985; Petrov, 1985; Dook et al., 1986, 1989; Smelov, 1989; Puchtel, 1992; Dobretsov et al., 1997; Jahn et al., 1998). The geological framework of the Olekma GGT is defined by the juxtaposition of the Olekma gneiss-migmatite complex and the Subgan granite-greenstone complex, which occur in the proportion 10:1. The Olekma gneiss-migmatite complex comprises tonalitic-trondhjemitic gneisses (TTG),

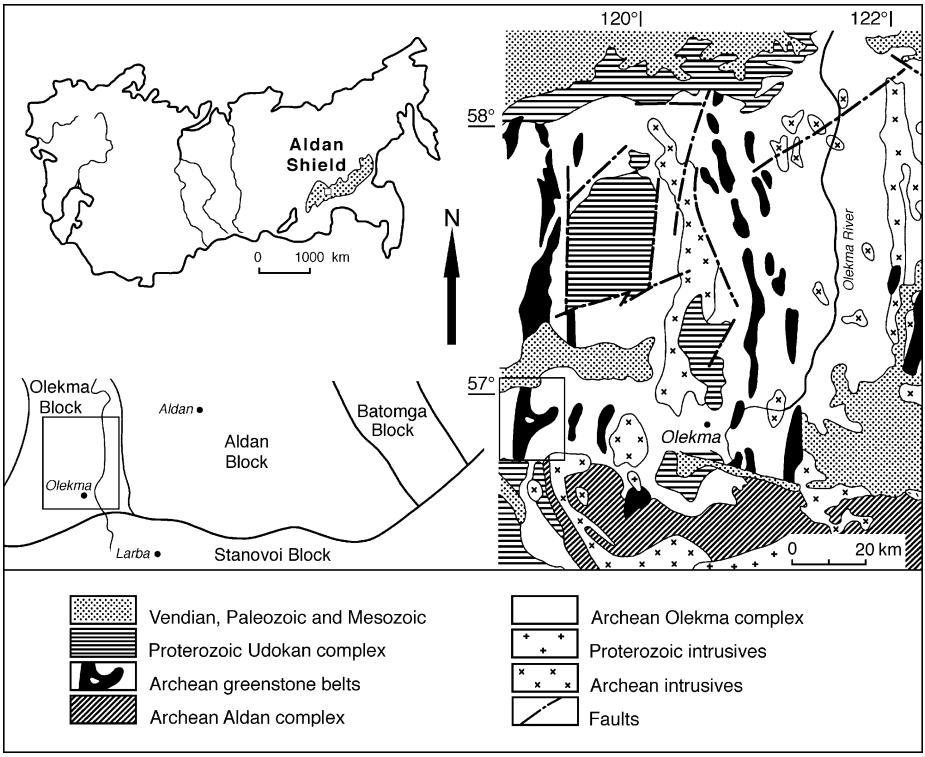

Fig. 1. Geological sketch map of the central part of the Aldan Shield (modified after Dook et al., 1986, 1989).

amphibolites, granitic gneisses and migmatites. Amphibolites and tonalite-trondhjemitic gneisses occur as remnants within vast areas of granitic gneisses. The U-Pb zircon ages of tonalite-trondhjemitic gneisses of 3212 ± 8, 3172 ± 24, and 3335 ± 2 Ma (Nutman et al., 1990, 1992; Jahn et al., 1998) and the Sm-Nd isochron age of 3235 ± 174 Ma (Puchtel et al., 1993) are considered to represent the time of emplacement of tonalite-trondhjemitic magmas. The granitic gneisses in the vicinity of the Olekma River range in age between 2.8 and 3.0 Ga, with most of the zircon data clustering around 3.0 Ga (Jahn et al., 1998). Puchtel et al. (1993) obtained a Sm-Nd isochron age of 2835 ± 94 Ma for these rocks, which is close to the U-Pb zircon (SHRIMP) age of 2862 ± 14 Ma (Baadsgaard et al., 1990). These ages reflect the time of high-grade metamorphic event and migmatitization.

The Subgan granite-greenstone complex includes sedimentary, volcaniclastic and volcanic rocks of greenstone belts, which have undergone polyphase greenschist to amphibolite facies deformation and metamorphism. The greenstone belts strike N-S and are confined to narrow linear zones (Fig. 1). Within these zones, the rocks of the Subgan complex are folded into narrow elongated troughs, and bounded by the highly schistose to blastomylonitic TTG of the Olekma complex. Various types of granites heal the tectonic contacts between the two complexes. The greenstone belts range in age between 3.2 and 2.7 Ga and can be subdivided into predominantly volcanic and volcano-sedimentary types on the basis of lithology. The Olondo greenstone belt is a typical example of the former group. It is arguably the best exposed and best studied among the greenstone belts in the Olekma GGT.

3. GEOLOGY OF THE OLONDO GREENSTONE BELT

The Olondo greenstone belt is located in the central part of the Olekma GGT. It is about 100 km long and has a maximum width of 30 km (Fig. 1). The geology and stratigraphy of the area has been described in a number of publications (e.g., Drugova et al., 1983, 1988; Popov et al., 1990, 1995; Puchtel, 1992; Dobretsov et al., 1992; Puchtel and Zhuravlev, 1993b). The belt occurs as narrow, dislocated and intricately deformed synforms with an approximately N-S trend. The largest, the Olondo synform, has a maximum size of about 30×10 km. It has steep limbs and splits up into two branches in its northern portion (Fig. 2). The Olondo synform is characterized by a rather symmetrical distribution of various volcanic rock types with respect to the axis of the V-shaped structure. Contacts between the supracrustal rocks and the surrounding tonalitic-trondhjemitic gneisses are tectonic. Numerous tonalite plutons intruded along the contacts between the TTG and the greenstone sequences. There are also several tonalite massifs in the central part of the synform. These plutons contain xenoliths of metamorphosed mafic-ultramafic to intermediate-felsic volcanic and plutonic rocks. The volcanic sequence of the belt has been subdivided into the lower and upper units (Puchtel and Zhuravlev, 1993b). The boundary between the two is not well defined geologically and is thus not shown on the map. The lower unit is exposed in the eastern and western marginal portions of the belt and has a

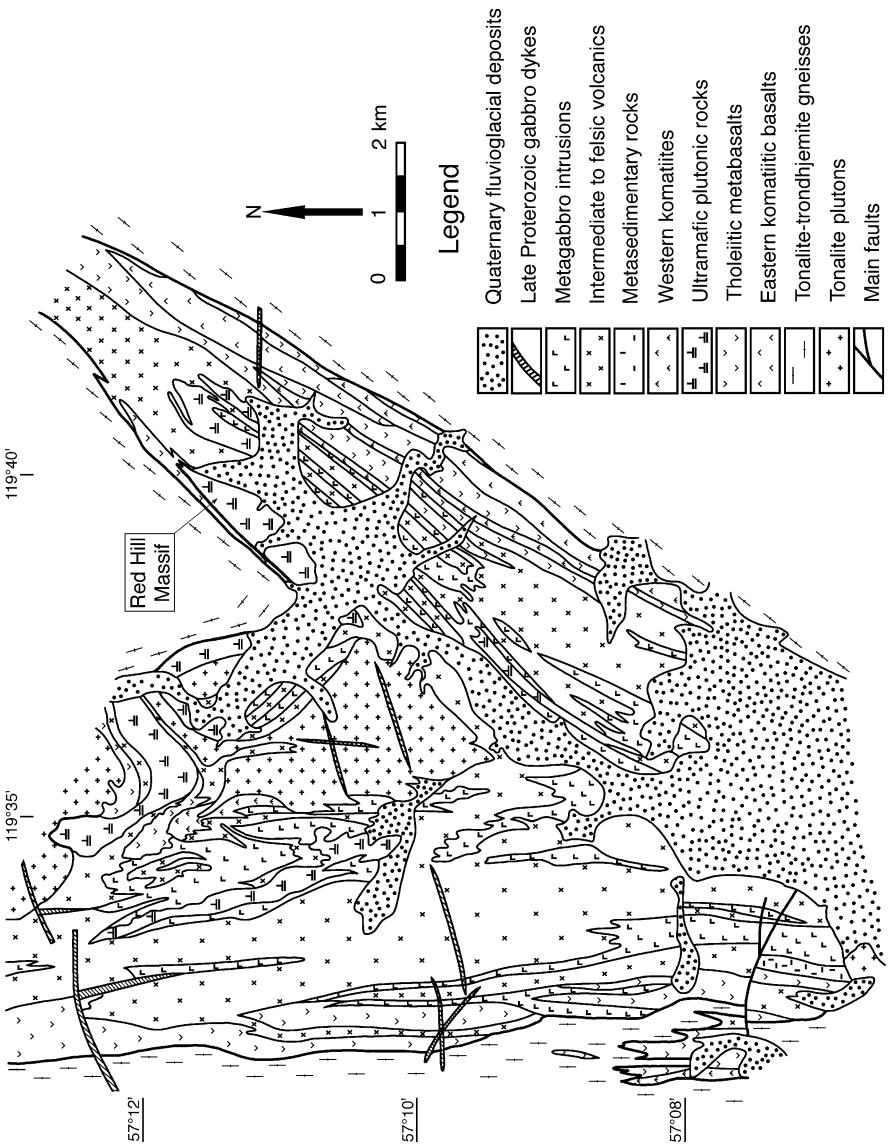

Fig. 2. Geologic-petrographical map of the Olondo greenstone belt.

maximum thickness of ~ 500 m. It is composed largely of mafic and ultramafic volcanic and volcaniclastic rocks. Volumetrically, the mafic metavolcanics are predominant. The upper unit occurs in the central part of the belt and consists of intermediate and felsic lavas and subvolcanic rocks with a subordinate amount of volcaniclastic lithologies and minor metasedimentary intercalations. The upper unit is about 600 m thick in total. Several authors opined that the above-mentioned succession of volcanic-sedimentary sequences cannot be regarded as having stratigraphic significance due to the intensive metamorphic reworking and deformations and the presence of numerous intrusive bodies of various compositions (Popov et al., 1995). Moreover, these authors suggest that the upper and lower sequences were spatially and temporary separated and were tectonically juxtaposed during later stages of evolution of the belt.

Mafic and ultramafic plutonic rocks constitute a substantial part (> 30%) of the Olondo complex. Ultramafic plutonic rocks are mostly represented by large dunite-peridotite bodies that have clear tectonic relationships with the country rocks. In most places they are confined to the contact between the lower and the upper unit rocks and locally occur within the lower unit lavas. Mafic plutonic rocks are most abundant in the belt. They are chiefly represented by differentiated gabbro sills that are confined to lithological boundaries.

The metamorphic grade ranges from epidote-amphibolite to amphibolite facies (T = 550–600 °C, P = 2–5 kbar) and increases slightly towards the margins of the belt (Drugova et al., 1983; Popov et al., 1990). Zircons from samples of felsic volcanics collected in the western part of the belt yielded a crystallization age of 2986 ± 12 Ma, those from the central part, 2998 ± 18 Ma, and zircons from the easternmost samples, 3005 ± 10 Ma (SHRIMP data: Baadsgaard et al., 1990). The greenstone belt is cut by metamorphosed dikes of picrites with a Sm-Nd whole-rock age of 2202 ± 41 Ma (Puchtel and Zhuravlev, 1993a).

The eastern branch of the synform (Fig. 2) is best preserved and contains several groups of mafic-ultramafic rocks of the lower unit, including Eastern komatiitic (EKB) and Eastern tholeiitic basalts (ETB), ultramafic plutonic rocks and gabbro sills, and thin horizons of actinolite-chlorite schists first identified as komatiites (here called Western komatiites) in the western branch of the synform by Drugova et al. (1988). Field characteristics and petrology of these rocks are given below. For more detailed information, the reader is referred to publications by Popov et al. (1990), Puchtel (1992), Puchtel and Zhuravlev (1993b).

4. FIELD PETROLOGY OF THE MAFIC AND ULTRAMAFIC ROCKS

4.1. Eastern Komatiitic Basalts

Eastern komatiitic basalts (EKB) form a gently dipping volcanic sequence consisting of massive, pillowed and differentiated lava flows 5.5 to 38 m thick which are underlain and overlain by tholeiitic basalts. The differentiated flows consist of the upper pillow, the middle massive, and the lower cumulate zone. The pillow lava zone is composed of closely

packed almost undeformed fragments a few tens of centimeter to a few meters in size. The fragments are tongue-like, bulbous, spheroidal or pillow-like in shape. Their tops are typically convex, and the bottoms either sag down into interpillow space, or are concave, conforming with the topography of the underlying fragments (Fig. 3). The matrix between the fragments is filled with a fine-grained actinolite-chlorite aggregate. The middle massive zone of the flows has a uniform structure and shows columnar jointing. The lower cumulate zone of the flows, where present, consists of a massive rock enriched in cumulate olivine now completely replaced by chlorite. Some of the thinner flows exhibit easily identified porous, brecciated tops and are composed of pillowed or massive komatiitic basalt throughout.

4.2. Eastern Tholeiitic Basalts (ETB) and Associated Gabbro

Tholeiitic basalts, now represented by amphibolite schists, occur as spatially separated volcanic sequences that underlie and overlie the komatiitic basalts. Where primary volcanic structures are preserved, it is possible to identify individual flows that vary in thickness from 5 to 50 m and have an amygdaloidal, massive or pillow structure. The amygdaloidal and massive flows have brecciated flowtops, which are made up of a highly porous, fragmented rock, the product of mechanical shattering of the upper chilled crust during the movement of the lava. In the massive flows, the flowtop breccia is underlain by a fine-grained amphibolite, that gives way to a coarser-grained variety. In the amygdaloidal flows, the amygdules decrease in size and abundance towards the bottom, with the lower third usually being massive. Pillow lava flows are composed of severely deformed fragments up to 2 m in size. Associated with the tholeiitic basalts are gabbro intrusions. They occur as concordant bodies, a few meters to several hundred meters thick, and are identified by symmetric chilled zones at the contacts with the country rocks, by relics of gabbro textures and a massive structure.

4.3. Western Komatiites

Western komatiites (WK) are now represented by series of concordant actinolite-chlorite schist bodies 0.5–25 m thick, which alternate with mafic lavas and tuffs. Due to their position in the lowermost part of the synform near the contact with TTG, the actinolite-chlorite schists are severely sheared, which obscures the nature of their precursor rock. Because of rather poor exposure, the exact dimensions of the bodies are not well known, but are presumed to be not less than several hundred to several thousand meters along the strike. At the inferred tops of some of the least altered bodies, rocks resembling flowtop breccias of komatiite lavas have been found. Those bodies might have been massive lava flows. Others, which lack evidence of extrusive origin, may represent hypabyssal sills.

4.4. Ultramafic Plutonic Rocks

Ultramafic plutonic rocks are represented by lenticular bodies of various size. The best preserved and best studied is the Red Hill massif exposed at the western flank of the eastern

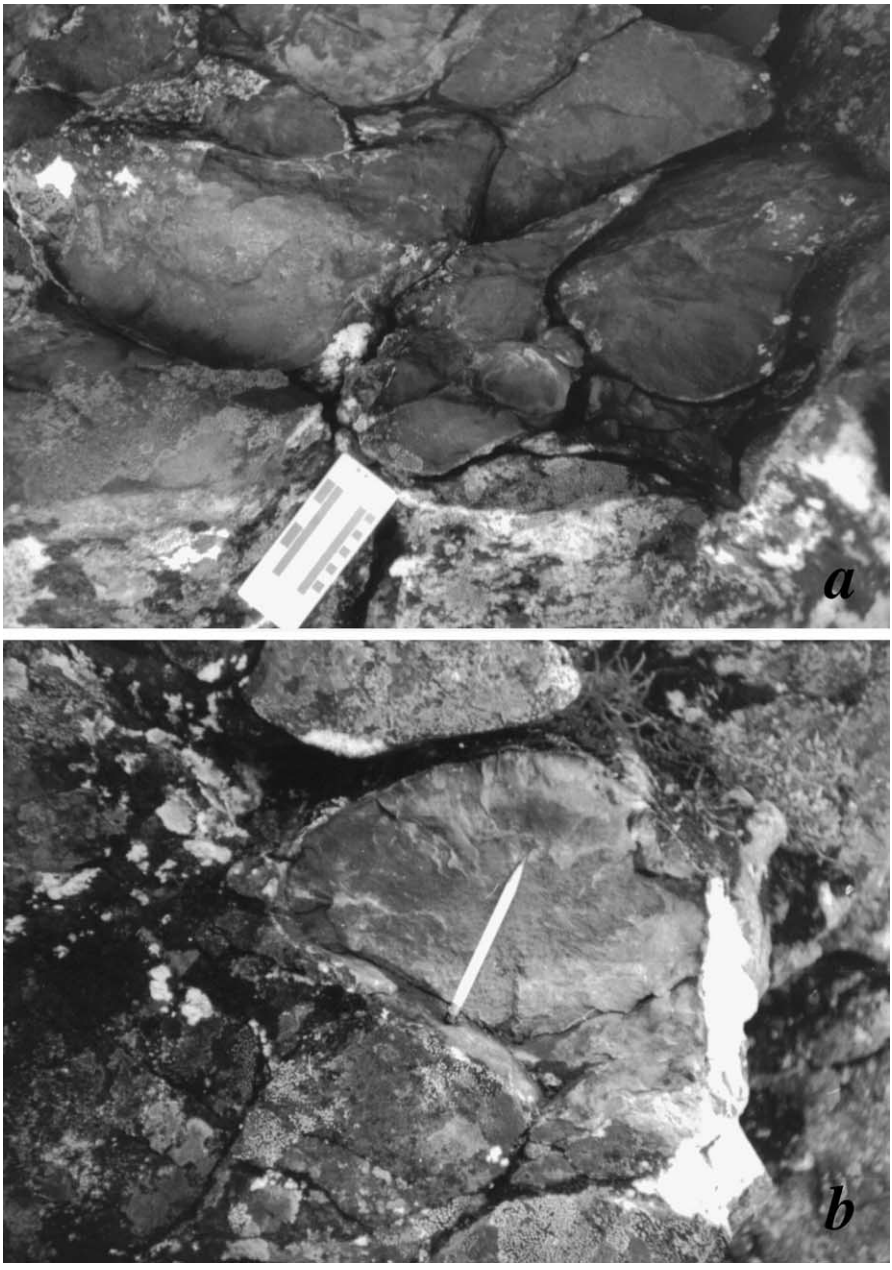

Fig. 3. Fragments of pillow lavas from the upper part of Eastern komatiitic basalt differentiated flows.

branch (Fig. 2). It is about 600 × 4000 m in size, and is concordant with the schistosity of the surrounding tholeiitic basalts. The body is cut into blocks by a series of faults and has had a long metamorphic and tectonic history. The western exposed contact is tectonic. The border zone is schistose near the contact and becomes massive a few meters away. The massif is composed of dunites-peridotites with relict igneous textures, and of products of their reworking, represented by metamorphic olivinites. The former occur in the least deformed central portion of the massif. The dunites are made up of 95–97% of equant, closely packed olivine grains 0.5–2 mm in size with a composition of $Fo_{91.2–92.4}$. The interstices are filled with clinopyroxene and chromite grains. The peridotites consist of 70–90% of elongate to equant euhedral olivine grains 1–8 mm in size, ranging in composition between $Fo_{89.9–90.5}$. Intercumulus minerals are represented by clinopyroxene and chromite grains. Typical features of the olivines from dunites and peridotites are their red-brown color, the ubiquitous presence of minute secondary mineral inclusions, lack of internal zoning and low Ca and Cr contents. Chromites from both dunites and peridotites contain 7–17% Al_2O_3, 4.5–6.5% MgO, and 44–52% Cr_2O_3, with $Cr\# = 0.82 \pm 0.05$ ($Cr\# = Cr/(Cr + Al)$). These chromite compositions plot in the field of boninites and island arc tholeiites, well above the field of MORBs as compiled by Portnyagin et al. (1997). As was also concluded by Dick and Bullen (1984), Cr# of greater than 0.7 are indicative of an arc-related rather than a MORB setting.

The olivinites consist of densely packed, bladed, and equant tabular olivine $Fo_{86.6–89.1}$ grains, 1–15 mm in size, elongated in the direction of the schistosity and showing a distinct cleavage coincident with the schistosity of the rocks and the amphibolites hosting the massif. Chromites from the olivinites are relatively high in Cr_2O_3 (39–42%), Al_2O_3 (5.7–12%), and MgO (2.7–4.6%), the contents of which, however, are lower than those in the original cumulate peridotites and dunites.

5. MAJOR AND TRACE ELEMENT GEOCHEMISTRY

The chemical compositions of mafic-ultramafic volcanic and intrusive rocks are shown in the primitive mantle normalized plots in Fig. 4, and representative analyses are listed in Table 1. Common features of basalts, komatiites and gabbros include LREE-depletions with $(La/Sm)_N$ ranging between 0.54 in WK and 0.96 in EKB, and pronounced positive U and Th anomalies in all rocks but ETB ($Nb/U = 12–20$ in EKB, WK and gabbro and ~ 28 in ETB as compared to the chondritic value of ~ 30). The $(Nb/Th)_N$ and $(Nb/La)_N$ ratios are on average also lower than chondritic (0.9 ± 0.2 and 0.8 ± 0.1, respectively).

5.1. Eastern Komatiitic Basalts

Eastern komatiitic basalts have a rather uniform MgO content of $15 \pm 1\%$ in the pillow zones of differentiated flows, which are considered to represent the composition of the emplaced lavas. They are substantially depleted in Al and Y relative to Ca and Ti and in

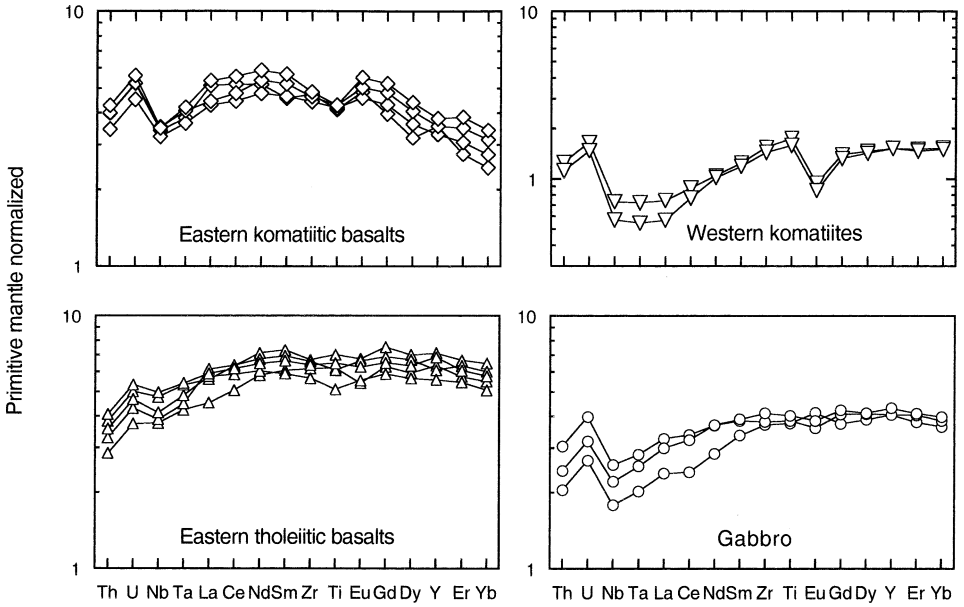

Fig. 4. Primitive mantle normalized abundances (Hofmann, 1988) of selected major and trace elements in the Olondo volcanic and plutonic rocks. Major and minor elements were determined by X-ray fluorescence spectrometry, REE by ID-TIMS, rest of trace elements by ICPMS.

Gd relative to Yb (Fig. 4), which led Puchtel and Zhuravlev (1993b) to classify them as belonging to the Al-depleted type of komatiitic rocks of Nesbitt et al. (1979). However, the rocks have pronounced negative Zr and Ti anomalies, which are not observed in pristine plume-related Al-depleted komatiites.

5.2. Western Komatiites

Western komatiites show nearly chondritic HREE distribution patterns of an Al-undepleted type komatiite (Fig. 4) and were classified as such by Puchtel and Zhuravlev (1993b). At the same time, these rocks have several chemical features that distinguish them from most Archean komatiites. First, they have about two times lower HFSE abundances at a given MgO content compared to typical plume-related komatiites such as those from the Kostomuksha or Abitibi greenstone belts (Arndt, 1986; Puchtel et al., 1998). Second, they are characterized by elevated Cr abundances (up to 4000 ppm), which correlate positively with MgO. This is in contrast to typical komatiites with $> 20\%$ MgO, in which Cr behaves as an incompatible element during lava differentiation (e.g., Arndt, 1986). Third, they have high Al/Ti ratios, about 27 on average, due to a relative Ti-depletion rather than Al-enrichment. Finally, they are enriched in SiO_2 (up to 51%) compared to typical komatiites with compa-

Table 1. Major and trace element data for mafic and ultramafic rocks from the Olondo greenstone belt

	Eastern komatiitic basalt				Eastern tholeiitic basalt					West komatiite		Gabbro			Red Hill massif		
Sample	07/2	07/6	07/9	07/16	109/1	507/4	104/1	105/1	106/2	8569	8551	15/1	15/2	86226	86245	86371	85358
SiO_2	48.2	49.5	50.7	49.0	48.8	48.9	49.2	49.0	49.5	46.7	49.6	49.5	49.1	46.2	40.4	41.0	41.6
TiO_2	0.78	0.78	0.76	0.75	1.17	0.93	1.10	1.27	1.12	0.29	0.32	0.73	0.70	0.67	0.08	0.07	0.04
$A1_2O_3$	7.83	7.93	7.70	7.72	15.3	15.2	14.6	14.8	15.2	7.12	7.21	14.5	14.2	14.6	1.24	1.24	0.76
Fe_2O_3	14.8	13.6	13.4	14.6	13.4	14.2	14.5	14.7	13.8	12.0	11.5	12.9	12.5	14.0	10.8	11.2	8.44
MnO	0.21	0.19	0.19	0.20	0.19	0.19	0.19	0.18	0.20	0.18	0.18	0.20	0.21	0.21	0.16	0.18	0.13
MgO	14.9	14.3	14.0	13.9	7.49	7.20	7.38	7.05	7.09	27.1	21.5	8.45	8.86	9.70	46.5	45.8	47.4
CaO	12.0	12.4	12.7	12.9	11.4	11.3	11.0	10.9	11.1	6.43	9.26	11.7	11.8	12.2	0.74	0.47	1.55
Na_2O	0.96	0.93	0.28	0.59	1.75	1.78	1.55	1.70	1.61	0.10	0.38	1.68	2.27	1.98	0.01	0.01	0.01
K_2O	0.12	0.14	0.14	0.11	0.26	0.13	0.33	0.20	0.16	0.02	0.04	0.10	0.19	0.22	0.01	0.01	0.01
P_2O_5	0.24	0.23	0.23	0.17	0.24	0.19	0.23	0.26	0.23	0.09	0.09	0.16	0.18	0.17	0.09	0.09	0.05
Cr	1692	1249	1320	1207	349	278	263	249	255	3519	2528	408	463	593	2672	5676	2244
Ni	518	370	397	356	137	112	120	108	129	1210	1095	131	155	170	3066	2762	3075
Zr	47	45	43	46	62	55	64	65	60	14	15	40	37	36			
Nb	2.15	2.18	1.99	2.11	3.07	2.56	2.40	2.94	2.32	0.350	0.450	1.36	1.59	1.10			
Ta	0.148	0.143	0.128	0.134	0.190	0.170	0.158	0.187	0.149	0.019	0.025	0.089	0.099	0.071			
Y	15	14	13	14	27	22	24	28	25	6	6	17	16	16			
Th	0.349	0.326	0.281	0.325	0.332	0.290	0.268	0.312	0.232	0.091	0.102	0.198	0.248	0.166			
U	0.114	0.107	0.092	0.106	0.108	0.095	0.087	0.102	0.076	0.030	0.033	0.065	0.081	0.054			
La	3.29	2.73	2.64	3.14	3.63	3.54	3.78	3.44	2.78	0.347	0.456	1.84	2.01	1.46	0.126	0.184	0.177
Ce	8.89	7.65	7.12	8.31	9.90	9.39	10.2	10.1	8.12	1.23	1.41	5.17	5.42	3.86	0.357	0.458	0.447
Nd	6.98	6.38	5.68	6.15	7.70	7.20	8.03	8.47	6.92	1.21	1.24	4.40	4.39	3.39	0.274	0.266	0.290
Sm	2.19	2.01	1.80	1.77	2.56	2.28	2.68	2.83	2.35	0.459	0.480	1.51	1.49	1.30	0.088	0.071	0.080
Eu	0.805	0.733	0.667	0.706	0.913	0.808	0.965	0.985	0.789	0.124	0.137	0.561	0.524	0.602	0.030	0.017	0.033
Gd	2.68	2.47	2.21	2.04	3.34	3.02	3.53	3.86	3.23	0.678	0.716	2.17	2.09	1.92	0.119	0.093	0.101
Dy	2.81	2.60	2.31	2.04	4.04	3.60	4.27	4.46	3.79	0.907	0.931	2.63	2.61	2.48	0.149	0.121	0.121
Er	1.61	1.46	1.28	1.15	2.53	2.27	2.64	2.78	2.39	0.611	0.626	1.71	1.69	1.58	0.103	0.096	0.080
Yb	1.42	1.30	1.14	1.01	2.39	2.10	2.49	2.68	2.28	0.621	0.634	1.65	1.60	1.51	0.115	0.120	0.083

Major elements in wt%, minor and trace elements in ppm. Analyses recalculated on an anhydrous basis.

rable MgO content. Therefore, though we continue to apply the term 'komatiite' to describe this rock type, we no longer consider them to be true komatiitic lavas.

5.3. Eastern Tholeiitic Basalts and Gabbros

Eastern tholeiitic basalts and gabbros both have unfractionated HREE patterns similar to those of Archean tholeiites and are thought to have been related by olivine-plagioclase-clinopyroxene fractionation (Puchtel and Zhuravlev, 1993b). Compared to typical Archean tholeiites (Condie, 1985; Arndt, 1991), however, they are higher in Ni, Co and Cr at a given MgO content and overall are substantially depleted in HFSE.

5.4. Dunites and Peridotites

Dunites and peridotites from the Red Hill massif have MgO contents ranging between 43 and 50% and were proposed to represent cumulates derived from the Western komatiite parental magma (Puchtel and Zhuravlev, 1993b). REE patterns vary from slightly depleted to enriched for both LREE and HREE. The abundances of moderately to highly incompatible elements are similar to those in residual ophiolitic peridotites (Jaques et al., 1983; Prinzhofer and Allegre, 1985) and are lower than those in ultramafic cumulates of thick differentiated komatiite lava flows (Arndt and Lesher, 1992).

6. PB AND ND ISOTOPE SYSTEMATICS

The Sm-Nd and Pb-Pb data for the Olondo mafic-ultramafic rocks are plotted in Figs. 5 and 6. In the Sm-Nd diagram, the data for the lavas (EKB + ETB) yield an isochron with an age of 3006 ± 84 Ma. This age is in good agreement with the results of ion-probe dating of zircons from different parts of the synform (2986 ± 12 to 3005 ± 10 Ma) and corresponds to the time of the eruption of the lavas. All samples have nearly uniform, positive initial εNd values ranging between $+2.5$ and $+2.8$.

Cumulate-textured dunites and peridotites of the Red Hill massif exhibit nearly chondritic Sm/Nd ratios; the data yield an isochron with an age of 3003 ± 117 Ma, identical to the emplacement age of the lavas. The initial εNd, however, is somewhat lower, at $+1.5 \pm 0.10$ (Fig. 5). Puchtel and Zhuravlev (1993b) interpreted these lower values as a result of hydrothermal alteration of the rocks, which has taken place nearly simultaneously with their emplacement.

In the $^{207}Pb/^{204}Pb$ vs $^{206}Pb/^{204}Pb$ diagram, the data for the mafic lavas also define an isochron with a slope corresponding to an age of 3065 ± 73 Ma, which is identical, within analytical uncertainty, to the Sm-Nd and zircon data. The μ_1, or time-integrated $^{238}U/^{204}Pb$ of the source of the magmas, is 8.76 ± 0.10, which is close to the mantle value of 8.75 at 3.0 Ga (Fig. 6). In the $^{208}Pb/^{204}Pb$ vs $^{206}Pb/^{204}Pb$ space, the data also define a linear trend, from which the Th/U ratio of the rocks is calculated to be 3.1 ± 0.3. This

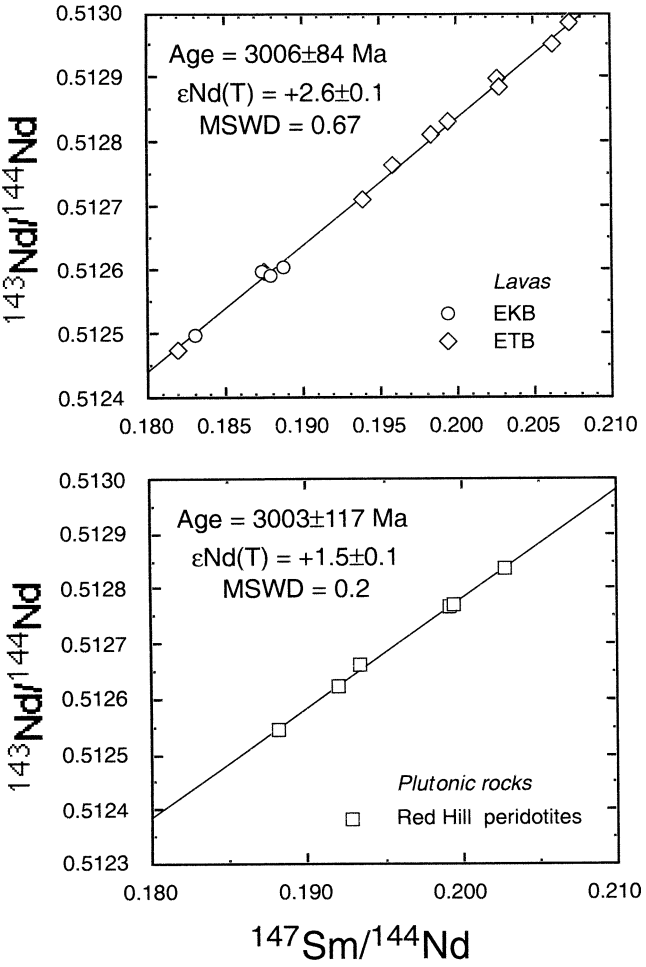

Fig. 5. Sm-Nd isochron diagrams for the Olondo volcanic rocks (top) and Red Hill massif dunites and peridotites (bottom). Analyses were carried out at the Max-Planck Institut für Chemie in Mainz using the technique described by Puchtel and Zhuravlev (1993b).

ratio is lower than that of the contemporary plume-derived mafic-ultramafic lavas from several greenstone belts of 3.3–3.4 (e.g., Dupré and Arndt, 1990; Lahaye and Arndt, 1996; Puchtel et al., 1998, 1999, and references therein). It is noteworthy that modern island arc lavas have Th/U ratios of around 2.5 (e.g., Thirlwall et al., 1996; Peate et al., 1997; Ewart et al., 1998).

In Fig. 7, compositions of the Olondo lavas are plotted on the diagram εNd vs Nb/Th, where the Nd isotopic compositions are recalculated relative to the hypothetical MOMO (major orogeny-mantle overturn) evolution line of Stein and Hofmann (1994). As can be

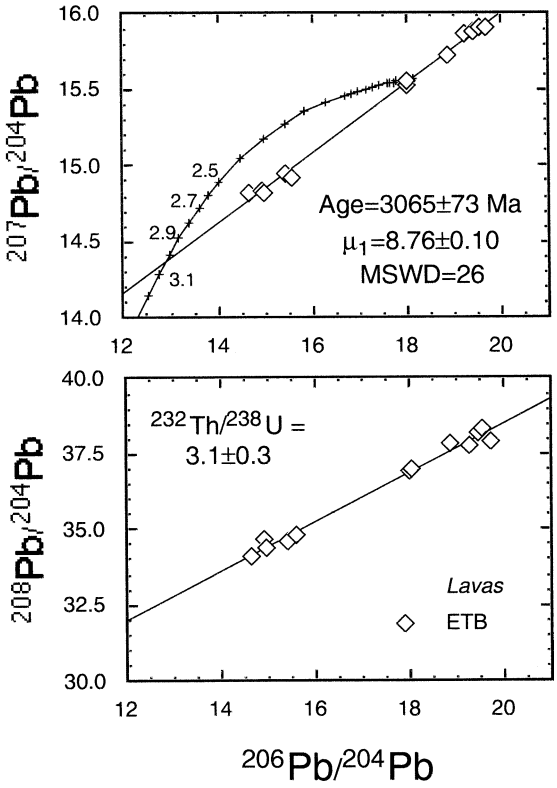

Fig. 6. Pb-Pb evolution diagrams for the Olondo volcanic rocks. The mantle evolution curve was drawn assuming a single-stage model, μ_1 value of 8.75, 4.50 Ga as the age of the Earth, and Canyon Diablo values of Tatsumoto et al. (1973) for the starting Pb isotopic composition. Analyses were carried out at the Max-Planck Institut für Chemie in Mainz using the technique described by Puchtel and Zhuravlev (1993b).

seen from the diagram, Eastern TB plot in the field of the Caribbean oceanic plateau basalts though at the lower end of Nb/Th ratios, while WK are associated with island arc volcanic rocks, and EKB and gabbros have intermediate compositions between the two.

7. RE-OS ISOTOPE SYSTEMATICS AND PGE GEOCHEMISTRY

Re-Os isotopic analyses were carried out on three bulk rock samples (Red Hill dunites and a peridotite) and two chromite separates, and the data are plotted on the Re-Os diagram in Fig. 8. All samples analyzed have high Os and very low Re abundances, and, thus, low Re/Os ratios, generally less than 0.1. This implies that the age corrections were minimal and have generally little effect on the measured Os isotopic compositions. All samples

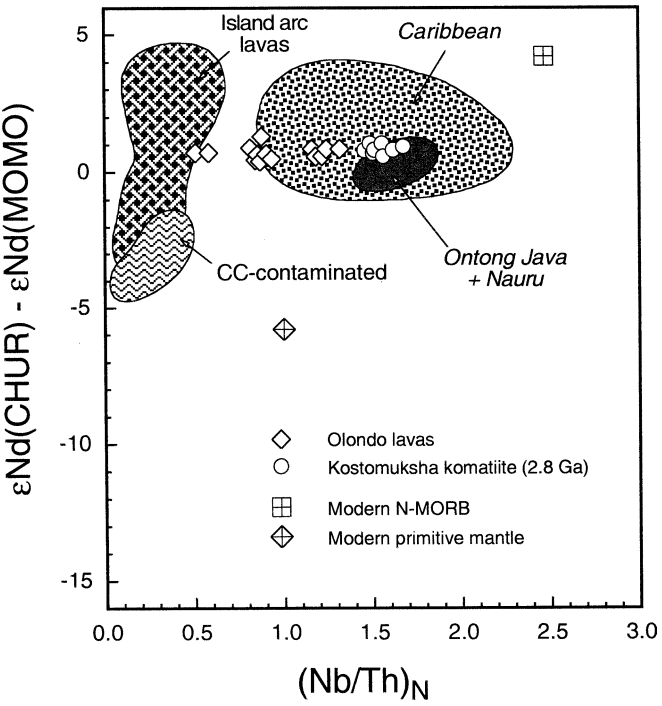

Fig. 7. $(Nb/Th)_N$ vs εNd(CHUR)-εNd(MOMO) data. The parameters of the PREMA reservoir are adapted from Wörner et al. (1986). ACC—average Archean continental crust of Rudnick and Fountain (1995); modern primitive mantle and N-MORB estimates are from Hofmann (1988). Nd isotopic compositions of ACC-contaminated rocks calculated at 2.7–2.5 Ga, and those of Olondo and Kostomuksha lavas at 3.0 and 2.8 Ga, respectively. The sources of the data used are available upon request.

plot close to the 3.0 Ga chondritic reference isochron and have an average initial γ^{187}Os (3.0 Ga) value of -0.5 ± 0.5. Since the chromites analyzed are magmatic in origin, and the bulk rocks mostly retain primary magmatic textures and mineralogy, this initial γ^{187}Os value is considered to reflect the Os isotopic composition of the mantle source of the rocks, even though they do not form an isochron in the Re-Os diagram. This initial value is within the range of Os isotopic compositions (from -5 to $+6$) obtained by Tsuru et al. (2000) and Walker et al. (1996, 2001) for Proterozoic and Phanerozoic ophiolites, mostly from supra-subduction zone (SSZ) settings.

PGE abundances in the Red Hill dunites and peridotites are plotted as CI-chondrite normalized values in Fig. 9. The patterns for the Olondo peridotites are similar to those for mantle rocks from SSZ-ophiolites (e.g., Rehkämper et al., 1997) and differ substantially from olivine cumulates in the lower parts of differentiated komatiite lava flows (e.g., Puchtel and Humayun 2000, 2001) in having higher Os, Ir and Ru contents and lower Pt and Pd abundances.

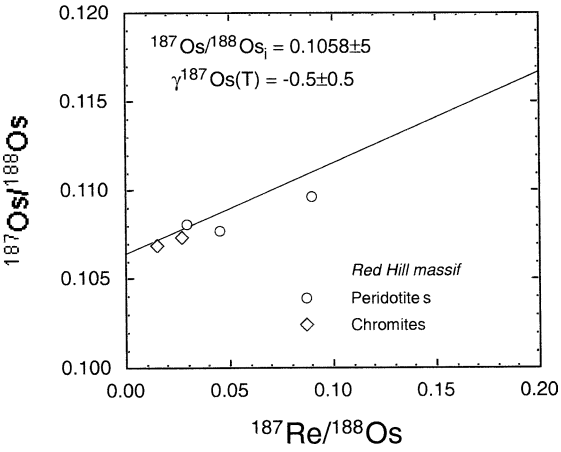

Fig. 8. Re-Os diagram for the Red Hill dunites, peridotites and chromite separates. The analyses were performed at the Max-Planck-Institut für Chemie in Mainz using the technique described in detail in Puchtel et al. (2001). The line represents the chondritic reference at 3.0 Ga.

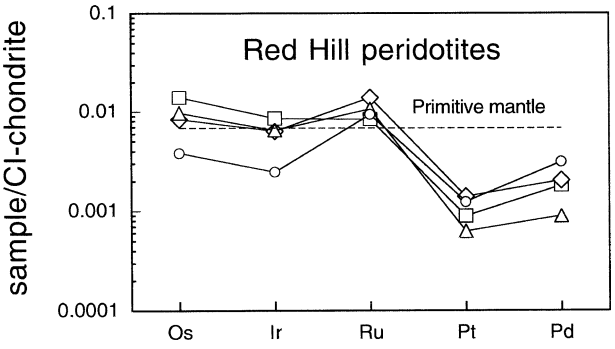

Fig. 9. PGE concentrations in the Red Hill dunites and peridotites normalized to CI-chondrite abundances of Anders and Grevesse (1989). The data were obtained using the Carius tube digestion ICPMS technique (Puchtel and Humayun, 2001).

8. TECTONIC SETTING OF THE OLONDO GREENSTONE BELT

Several lines of evidence suggest that the Olondo greenstone belt represents a fragment of an ancient suprasubduction zone ophiolite sequence.

1. Submarine supracrustal sequences of the Olondo greenstone belt have linear rather than areal distribution. This favors their origin in a subduction zone environment and not as part of an Archean oceanic plateau. Unlike Phanerozoic ophiolite complexes, which

include sheeted dike complex, the Olondo sequence is characterized by the presence of a large amount of mafic and ultramafic sills. This may be indicative of a greater magma supply and faster spreading rates in the Archean, as suggested by, e.g., Saunders et al. (1996).

2. Olondo mafic-ultramafic lavas and gabbros have geochemical signatures typical of boninite-like rocks in Phanerozoic SSZ-ophiolite sequences. These include depletions in HFSE and enrichments in Si and Cr at a given MgO content, which point to a mantle source that experienced a previous history of melt depletion, and enrichments in Th and U, typical of subduction-related magmas (e.g., Taylor et al., 1994; Smellie et al., 1995; Portnyagin et al., 1997, and references therein). These features coupled with the LREE- and Nd-Pb depleted mantle-type characteristics are not observed in oceanic plateau or MORB lavas and are unique to SSZ ophiolite sequences.

3. The presence of high-Mg lavas such as the Western komatiites and Eastern komatiitic basalts with boninite-like geochemical and isotopic signatures indicates greater degrees of mantle melting above a subduction zone induced by fluids from a downgoing slab having lowered the melting point. This process is argued to produce SSZ ophiolite complexes with depleted mantle sequences and thicker ultramafic crustal sections (e.g., Pearce et al., 1984), in contrast to dry and less extensive melting beneath oceanic ridges, which produces undepleted mantle lherzolite and no ultramafic crustal sections.

4. PGE distribution patterns in the Red Hill massif dunites and peridotites are typical of mantle rocks from SSZ environments. They were derived from a source previously depleted in incompatible Pt and Pd.

5. The average initial γOs of -0.5 ± 0.5 for bulk rock dunite-peridotite samples and chromite separates is regarded as reflecting the Os isotopic composition of the Archean convecting upper mantle in the region. These data allow to trace the evolution of the Os isotopic composition of the convecting upper mantle as far back in the Earth history as the middle Archean.

REFERENCES

Anders, E., Grevesse, N., 1989. Abundances of the elements: Meteoritic and solar. Geochimica et Cosmochimica Acta 53, 197–214.

Arndt, N.T., 1986. Differentiation of komatiite flows. Journal of Petrology 27, 279–301.

Arndt, N.T., 1991. High Ni in Archaean tholeiites. Tectonophysics 187, 411–420.

Arndt, N.T., Lesher, C.M., 1992. Fractionation of REE's by olivine and the origin of Kambalda komatiites, Western Australia. Geochimica et Cosmochimica Acta 56, 4191–4204.

Baadsgaard, H., Nutman, A.P., Samsonov, A.V., 1990. Geochronology of the Olondo greenstone belt. ICOG-7, 6.

Condie, K.C., 1985. Secular variation in the composition of basalts: An index to mantle evolution. Journal of Petrology 26, 545–563.

Condie, K.C., 1995. Episodic ages of greenstones: A key to mantle dynamics? Geophysical Research Letters 22, 2215–2218.

Condie, K.C., 1998. Episodic continental growth and supercontinents: A mantle avalanche connection? Earth and Planetary Science Letters 163, 97–108.

deWit, M.J., Ashwal, L.D., 1986. Workshop on tectonic evolution of greenstone belts. LPI, Technical Report 86-10, Houston, TX.

deWit, M.J., Ashwal, L.D., 1997. Greenstone Belts. In: Oxford Monographs on Geology and Geophysics, vol. 35, p. 809.

Dick, H.J.B., Bullen, T., 1984. Chromian spinel as a petrogenetic indicator in abyssal and alpine-type peridotites and spatially associated lavas. Contributions to Mineralogy and Petrology 86, 54–76.

Dobretsov, N.L., Konnikov, E.G., Dobretsov, N.N., 1992. Precambrian ophiolite belts of southern Siberia, Russia, and their metallogeny. Precambrian Research 58, 427–446.

Dobretsov, N.N., Popov, N.V., Smelov, A.P., Bogomolova, L.M., Moskovchenko, N.I., Barton, J.M., 1997. The Aldan-Stanovik Shield. In: deWit, M.J., Ashwal, L.D. (Eds.), Greenstone Belts. In: Oxford Monographs on Geology and Geophysics, vol. 35, pp. 710–725.

Dook, V.L., Kitsul, V.I., Petrov, A.F., 1986. The Early Precambrian of South Yakutia. Nauka, Moscow, p. 280.

Dook, V.L., Neymark, L.A., Rudnik, V.A., Kröner, A., 1989. The oldest rocks of the Aldan-Stanovik Shield, Eastern Siberia, USSR. Excursion guide for geological field trip to the Aldan-Stanovik Shield. Leningrad, Mainz, p. 121.

Drugova, G.M., Bushmin, S.A., Sochava, A.V., Savel'eva, T.E., Kharitonov, A.L., 1985. Trough complexes of the western part of the Aldan Shield. In: Kuznetsov, V.A. (Ed.), Precambrian trough Structures of the BAM Region and Their Metallogeny. Nauka, Novosibirsk, pp. 102–111.

Drugova, G.M., Kharitonov, A.L., Bushmin, S.A., Chukhonin, A.P., Shuleshko, I.K., 1983. Structural-Metamorphic Development of the Olondo Complex (E. Siberia). Nauka, Leningrad, pp. 49–65.

Drugova, G.M., Puchtel, I.S., Shustova, L.Y., Berezhnaya, N.G., 1988. The Olondo greenstone belt, Aldan Shield. Izvestiya Akademii Nauk SSSR 8, 40–56.

Dupré, B., Arndt, N.T., 1990. Pb isotopic composition of Archean komatiites and sulfides. Chemical Geology 85, 35–56.

Ewart, A., Collerson, K.D., Regelous, M., Wendt, J.I., Niu, Y., 1998. Geochemical evolution within the Tonga-Kermadec Lau arc back-arc systems: The role of varying mantle wedge composition in space and time. Journal of Petrology 39, 331–368.

Hofmann, A.W., 1988. Chemical differentiation of the Earth: The relationship between mantle, continental crust and oceanic crust. Earth and Planetary Science Letters 90, 297–314.

Jahn, B.M., Gruau, G., Capdevila, R., Cornichet, J., Nemchin, A., Pidgeon, R., Rudnik, V.A., 1998. Archaean crustal evolution of the Aldan Shield, Siberia: Geochemical and isotopic constraints. Precambrian Research 91, 333–363.

Jaques, A.L., Chappell, B.W., Taylor, S.R., 1983. Geochemistry of cumulus peridotites and gabbros from the Marum ophiolite complex, Northern Papua New Guinea. Contributions to Mineralogy and Petrology 83, 154–164.

Lahaye, Y., Arndt, N.T., 1996. Alteration of a komatiite flow from Alexo, Ontario. Journal of Petrology 37, 1261–1284.

Mironiuk, E.P., Liubimov, V.K., Magnushevsky, E.L., 1971. Geology of the Western Aldan Shield. Nedra, Moscow, p. 237.

Nesbitt, R.W., Sun, S.S., Purvis, A.C., 1979. Komatiites: Geochemistry and genesis. Canadian Mineralogist 17, 165–186.

Nutman, A.P., Chernyshev, I.V., Baadsgaard, H., Smelov, A.P., 1992. The Aldan Shield of Siberia, USSR: The age of its Archean components and evidence for widespread reworking in the mid-Proterozoic. Precambrian Research 54, 195–210.

Nutman, A.P., Chernyshev, I.V., Baadsgaard, H., 1990. The Archean Aldan Shield of Siberia, USSR: The search of its oldest rocks and evidence for reworking in the Mid-Proterozoic. In: Third International Archaean Symposium, p. 27.

Pearce, J.A., Lippard, S.J., Roberts, S., 1984. Characteristics and tectonic significance of supra-subduction zone ophiolites. In: Kokelaar, B.P., Howells, M.F. (Eds.), Marginal Basin Geology. Geological Society Special Publication, 77–94.

Peate, D.W., Pearce, J.A., Hawkesworth, C.J., Colley, H., Edwards, C.M.H., Hirose, K., 1997. Geochemical variations in Vanuatu arc lavas: The role of subducted material and a variable mantle wedge composition. Journal of Petrology 38, 1331–1358.

Petrov, A.F., 1985. Tectonic setting of Precambrian greenstone belts in the Aldan Shield structure. In: Kuznetsov, V.A. (Ed.), Precambrian Trough Structures of the BAM Region and Their Metallogeny. Nauka, Novosibirsk, pp. 90–96.

Popov, N.V., Dobretsov, N.N., Smelov, A.P., Bogomolova, L.M., 1995. Tectonics, metamorphism and the problems of evolution of the Olondo greenstone belt. Petrology 3, 73–86.

Popov, N.V., Smelov, A.P., Dobretsov, N.N., Bogomolova, L.M., Kartavchenko, V.G., 1990. The Olondo Greenstone Belt. Yakutsk Scientific Center, Yakutsk, p. 172.

Portnyagin, M.V., Danyushevsky, L.V., Kamenetsky, V.S., 1997. Coexistence of two distinct mantle sources during formation of ophiolites: A case study of primitive pillow lavas from the lowest part of the volcanic section of the Troodos ophiolite, Cyprus. Contributions to Mineralogy and Petrology 128, 287–301.

Prinzhofer, A., Allegre, C.J., 1985. Residual peridotites and mechanisms of partial melting. Earth and Planetary Science Letters 74, 251–265.

Puchtel, I.S., 1992. Petrology of mafic-ultramafic rocks and evolution of the crust-mantle system in the early Precambrian of the Olekma gneiss-greenstone terrain, Aldan Shield. Ph.D. thesis. Institute of Ore Deposit Geology, Petrology, Mineralogy and Geochemistry, Moscow, p. 256.

Puchtel, I.S., Bogatikov, O.A., Simon, A.K., 1993. The Early Precambrian crust-mantle evolution of the Olekma gneiss-greenstone terrane, Aldan Shield. Petrology 1, 451–473.

Puchtel, I.S., Brügmann, G.E., Hofmann, A.W., 2001. ^{187}Os-enriched domain in an Archaean mantle plume: Evidence from 2.8 Ga komatiites of the Kostomuksha greenstone belt, NW Baltic Shield. Earth and Planetary Science Letters 186, 513–526.

Puchtel, I.S., Hofmann, A.W., Mezger, K., Jochum, K.P., Shchipansky, A.A., Samsonov, A.V., 1998. Oceanic plateau model for continental crustal growth in the Archaean: A case study from the Kostomuksha greenstone belt, NW Baltic Shield. Earth and Planetary Science Letters 155, 57–74.

Puchtel, I.S., Hofmann, A.W., Amelin, Y.V., Garbe-Schönberg, C.-D., Samsonov, A.V., Shchipansky, A.A., 1999. Combined mantle plume-island arc model for the formation of the 2.9 Ga Sumozero-Kenozero greenstone belt, SE Baltic Shield: Isotope and trace element constraints. Geochimica et Cosmochimica Acta 63, 3579–3595.

Puchtel, I.S., Humayun, M., 2000. Platinum group elements in Kostomuksha komatiites and basalts: Implications for oceanic crust recycling and core-mantle interaction. Geochimica et Cosmochimica Acta 64, 4227–4242.

Puchtel, I.S., Humayun, M., 2001. Platinum group element fractionation in a komatiitic basalt lava lake. Geochimica et Cosmochimica Acta 65, 2979–2993.

Puchtel, I.S., Zhuravlev, D.Z., 1993a. Nd-isotope systematics and petrogenesis of the early Proterozoic picrites in the Olekma granite-greenstone region. Geochemistry International 30, 37–49.

Puchtel, I.S., Zhuravlev, D.Z., 1993b. Petrology of mafic-ultramafic metavolcanics and related rocks from the Olondo greenstone belt, Aldan Shield. Petrology 1, 308–348.

Rehkämper, M., Halliday, A.N., Barfod, D., Fitton, J.G., 1997. Platinum-group element abundance patterns in different mantle environments. Science 278, 1595–1598.

Rudnick, R.L., Fountain, D.M., 1995. Nature and composition of the continental crust: A lower crustal perspective. Reviews of Geophysics 33, 267–309.

Saunders, A.D., Tarney, J., Kerr, A.C., Kent, R.W., 1996. The formation and fate of large oceanic igneous provinces. Lithos 37, 81–95.

Smellie, J.L., Stone, P., Evans, J., 1995. Petrogenesis of boninites in the Ordovician Ballantrae Complex ophiolite, southwestern Scotland. Journal of Volcanology and Geothermal Research 69, 323–342.

Smelov, A.P., 1989. Metamorphic Evolution of the Olekma Granite-Greenstone Terrain. Nauka, Novosibirsk, p. 128.

Stein, M., Hofmann, A.W., 1994. Mantle plumes and episodic crustal growth. Nature 372, 63–68.

Tatsumoto, M., Knight, R.J., Allègre, C.J., 1973. Time differences in the formation of meteorites as determined from the ratio of lead 207 to lead 206. Science 180, 1279–1283.

Taylor, R.N., Nesbitt, R.W., Vidal, P., Harmon, R.S., Auvray, B., Croudace, I.W., 1994. Mineralogy, chemistry, and genesis of the boninite series volcanics, Chichijima, Bonin-Islands, Japan. Journal of Petrology 35, 577–617.

Thirlwall, M.F., Graham, A.M., Arculus, R.J., Harmon, R.S., Macpherson, C.G., 1996. Resolution of the effects of crustal assimilation, sediment subduction, and fluid transport in island arc magmas: Pb-Sr-Nd-O isotope geochemistry of Grenada, Lesser Antilles. Geochimica et Cosmochimica Acta 60, 4785–4810.

Tsuru, A., Walker, R.J., Kontinen, A., Peltonen, P., Hanski, E., 2000. Re-Os isotopic systematics of the 1.95 Ga Jormua Ophiolite Complex, northeastern Finland. Chemical Geology 164, 123–141.

Wörner, G., Zindler, A., Staudigel, H., Schmincke, H.-U., 1986. Sr, Nd, and Pb isotope geochemistry of Tertiary and Quaternary alkaline volcanics from West Germany. Earth and Planetary Science Letters 79, 107–119.

Walker, R.J., Hanski, E., Vuollo, J., Liipo, J., 1996. The Os isotopic composition of Proterozoic upper mantle: Evidence for chondritic upper mantle from the Outokumpu ophiolite, Finland. Earth and Planetary Science Letters 141, 161–173.

Walker, R.J., Prichard, H.M., Ishivatari, A., Pimentel, M., 2001. The osmium isotopic composition of the convecting upper mantle deduced from ophiolite chromites. Geochimica et Cosmochimica Acta 66, 329–345.